PNAS RESEARCH ARTICLE | NEUROSCIENCE

Retromer dysfunction in amyotrophic lateral sclerosis

Eduardo J. Pérez-Torres[a,b], Irina Utkina-Sosunova[b,c], Vartika Mishra[a,b], Peter Barbuti[b,c], Mariangels De Planell-Saguer[a,b], Georgia Dermentzaki[a,b], Heather Geiger[d], Anna O. Basile[d], Nicolas Robine[d], Delphine Fagegaltier[e], Kristin A. Politi[a,b], Paola Rinchetti[a,b], Vernice Jackson-Lewis[a,b,c], NYGC ALS Consortium[1], Matthew Harms[c,f], Hemali Phatnani[b,c,e], Francesco Lotti[a,b], and Serge Przedborski[a,b,c,g,2]

Edited by Ana Maria Cuervo, Albert Einstein College of Medicine, Bronx, NY; received October 12, 2021; accepted May 3, 2022

Retromer is a heteropentameric complex that plays a specialized role in endosomal protein sorting and trafficking. Here, we report a reduction in the retromer proteins—vacuolar protein sorting 35 (VPS35), VPS26A, and VPS29—in patients with amyotrophic lateral sclerosis (ALS) and in the ALS model provided by transgenic (Tg) mice expressing the mutant superoxide dismutase-1 G93A. These changes are accompanied by a reduction of levels of the α-amino-3-hydroxy-5-methyl-4-isoxazolepropionic acid receptor subunit GluA1, a proxy of retromer function, in spinal cords from Tg SOD1^{G93A} mice. Correction of the retromer deficit by a viral vector expressing *VPS35* exacerbates the paralytic phenotype in Tg SOD1^{G93A} mice. Conversely, lowering *Vps35* levels in Tg SOD1^{G93A} mice ameliorates the disease phenotype. In light of these findings, we propose that mild alterations in retromer inversely modulate neurodegeneration propensity in ALS.

ALS | retromer | neurodegeneration

Significance

Amyotrophic lateral sclerosis is an adult-onset paralytic disorder whose mechanism remains uncertain. In this work, we report a defect in the retromer complex, which plays a crucial role in endosomal protein sorting and trafficking in this fatal neurological disease. We found that restoring retromer expression in a mouse model of the disease aggravates the paralytic phenotype, whereas reducing retromer expression has the opposite beneficial effect. Our study sheds light on a role for retromer in neurodegeneration of pathogenic and therapeutic importance.

The retromer complex mediates the sorting and trafficking of proteins within the endolysosomal pathway (1). It is composed of two main functional subcomplexes: the cargo-selective trimer of vacuolar protein sorting 26 (VPS26)–VPS29–VPS35 and a membrane-bending dimer of sorting nexins (SNXs) (1). The retromer is essential to the cell physiology as evidenced by the fact that ablation of *Vps35* or *Vps26* is embryonically lethal in mice (2).

Retromer dysfunction has been identified in multiple neurodegenerative diseases. For instance, decreased levels of VPS35 mRNA, and of VPS35 and VPS26 proteins have been reported in the medial temporal lobe of patients with Alzheimer's disease (AD) (3). Decreased levels of the retromer constituents were also reported in postmortem tissues from patients with different Parkinsonian syndromes, including Parkinson's disease (PD), Down's syndrome (DS), and Pick's tauopathy (3–6). Moreover, AD, PD, and DS experimental models recapitulate these retromer alterations (5, 7, 8). Support for a role of retromer defect in neurodegeneration comes from the demonstrations of partial loss-of-function (LOF) mutations in VPS35 that are linked to PD (9–13). Despite the increased recognition of retromer defects in neurodegenerative disorders such as PD and AD, little is still known about the status and potential contribution of retromer to motor neuron (MN) diseases such as amyotrophic lateral sclerosis (ALS) (14)—a common paralytic disorder in adults (15) that causes proportionally much higher disability and fatality rates than PD and AD (16, 17).

Here, we report dysregulation of VPS35, VPS26A, and VPS29 in postmortem tissues both from ALS patients and from transgenic mice expressing mutant superoxide dismutase-1 G93A (Tg SOD1^{G93A}), which is a model of the disease that is used extensively (18). Specifically, we found a reduction of these core retromer proteins in symptomatic Tg SOD1^{G93A} mice in tissues from the nervous system but not from nonneural tissues. We found that overexpressing VPS35 by viral vector enhanced the ALS-like phenotype in Tg SOD1^{G93A} mice, and conversely, further reducing Vps35 had the opposite effects. In light of these findings, we searched for putative LOF polymorphisms in retromer-related genes, which allowed us to exclude that depletion of such genetic variants in retromer genes is a strong risk factor for developing ALS. Collectively, our findings suggest that a mild reduction in retromer function may attenuate neurodegeneration by modulating the expression of factors that contribute to the susceptibility of MNs, the main cellular target of the disease process. Consequently, therapies aiming at increasing retromer expression in ALS may have to be considered with cautions.

Results

Dysregulation of Retromer Subunits in Human ALS and Control Brain Tissues and Cell Types. To investigate the role for retromer in ALS pathogenesis, we first compared expression of the 107 genes that make up the Harmonizome Retromer Complex Gene

Author affiliations: [a]Department of Pathology and Cell Biology, Columbia University Irving Medical Center, New York, NY 10032; [b]Center for Motor Neuron Biology and Diseases, Columbia University Irving Medical Center, New York, NY 10032; [c]Department of Neurology, Columbia University Irving Medical Center, New York, NY 10032; [d]Computational Biology, New York Genome Center, New York, NY 10013; [e]Center for Genomics of Neurodegenerative Disease, New York Genome Center, New York, NY 10013; [f]Institute for Genomic Medicine, Columbia University Irving Medical Center, New York, NY 10032; and [g]Department of Neuroscience, Columbia University, New York, NY 10027

Author contributions: E.J.P.-T., V.M., P.B., G.D., D.F., M.H., H.P., F.L., and S.P. designed research; E.J.P.-T., I.U.-S., V.M., P.B., M.D.P.-S., G.D., K.A.P., P.R., V.J.-L., M.H., F.L., and S.P. performed research; H.G., A.O.B., N.R., D.F., N.Y.G.C.A.L.S.C., H.P., and F.L. contributed new reagents/analytic tools; E.J.P.-T., I.U.-S., P.B., M.D.P.-S., H.G., A.O.B., N.R., D.F., K.A.P., P.R., V.J.-L., M.H., F.L., and S.P. analyzed data; and E.J.P.-T., I.U.-S., V.M., P.B., H.G., D.F., V.J.-L., M.H., H.P., F.L., and S.P. wrote the paper.

The authors declare no competing interest.

This article is a PNAS Direct Submission.

[1]A complete list of the NYGC ALS Consortium group can be found in the *SI Appendix*.

[2]To whom correspondence may be addressed. Email: sp30@columbia.edu.

This article contains supporting information online at http://www.pnas.org/lookup/suppl/doi:10.1073/pnas.2118755119/-/DCSupplemental.

Published June 24, 2022.

Set (HRCGS; https://maayanlab.cloud/Harmonizome/gene_set/retromer+complex/COMPARTMENTS+Text-mining+Protein+Localization+Evidence+Scores) in the spinal cord of 482 ALS cases vs. 118 normal controls (Dataset S1) using bulk ribonucleic acid sequencing (RNA-seq) data from the New York Genome Center (NYGC) ALS Consortium (*Materials and Methods*). Of the 107 HRCGSs (Dataset S2), 105 were expressed in the spinal cord, and 2 (i.e., *PIGR* and *PTCHD3*) were not detected. Of those that were detected, over 80% (i.e., 87 genes) were significantly dysregulated (false discovery rate [FDR] < 0.01) in ALS compared with controls, with changes ranging from a 39% decrease to a 52% increase in ALS in *TF* and *LRRK2* transcripts, respectively (Fig. 1*A* and Dataset S2). Notably, we observed significant up-regulation (FDR < 1.0E-16) of key retromer components, including VPS29, VPS35, and VPS26A as well as SNX2, SNX3, and SNX5 mRNAs (each increased by >25% in ALS).

To determine the cellular origin of the observed retromer alterations in ALS, we turned to cultured human cells by focusing on the two cell types relevant to the disease: human primary astrocytes and MNs generated from induced pluripotent stem cells (iPSC-MNs) from ALS patients carrying SOD1 mutations (mutSOD1). The focus on these two selected cell types was prompted by the fact that astrocytes are not only the predominant nonneuronal cell types in the CNS (central nervous system), but also thought to contribute to ALS pathogenesis (19), and that MNs are the main target of the ALS degenerative process (15). Of note, while cultured astrocytes can be generated from postmortem samples and both mutSOD1 and gene-negative ALS astrocytes are found to exert comparable deleterious effects on neighboring MNs (20), production of human MNs, however, is thus far only possible through differentiation from stem cells such as induced pluripotent stem cells (iPSCs), whose ALS-like phenotype is brought about by the expression of ALS-related gene mutations, like mutSOD1 (21). We established cultured human astrocytes from patients with ALS and subjects without neurological disorder as before (20). Detection by real-time quantitative reverse transcription polymerase chain reaction (qRT-PCR) revealed that levels of VPS35, VPS26A, and VPS29 messenger ribonucleic acids (mRNAs) were significantly increased in astrocytes from ALS patients compared with control subjects (*SI Appendix*, Fig. S1*A*). Conversely, VPS35, VPS26A, and VPS29 protein levels were lower in human ALS astrocytes with small to large effect size for VPS26A (d = 0.29), VPS29 (d = 0.30), and VPS35 (d = 1.74) (Fig. 1*B*). As for the iPSC-MNs, which were produced as before (22) and studied at 14 d in vitro (DIV), VPS35, VPS26A, and VPS29 mRNA levels were comparable in human mutSOD1 iPSC-MNs and wild-type iPSC-MNs (*SI Appendix*, Fig. S1*B*). In contrast, protein contents were decreased in human mutSOD1 iPSC-MNs compared with wild-type iPSC-MNs, with medium to large effect size for VPS26A (d = 0.65), VPS29 (d = 1.88), and VPS35 (d = 3.89) (Fig. 1*C*). Thus, astrocytes and iPSC-MNs from ALS patients show a reduction of retromer proteins, with no corresponding reduction in mRNA levels.

Retromer Expression Is Decreased in Tg SOD1^{G93A} Mice Neural Tissues. Given the observed retromer changes in brain tissues and cells from ALS patients, we posited that these molecular alterations may contribute to the neurodegenerative process. To begin addressing this question, we first asked whether Tg SOD1^{G93A} mice, a commonly used preclinical model for testing for mechanistic and therapeutic hypotheses of ALS, also present with retromer subunit alterations. Spinal cords from Tg SOD1^{G93A} mice were collected at three specific time points: postnatal day 60 (P60) for bulk and P30 for spatial transcriptomic or presymptomatic stage, P90 or early symptomatic stage, and P120 or advanced symptomatic stage. By qRT-PCR, we found no

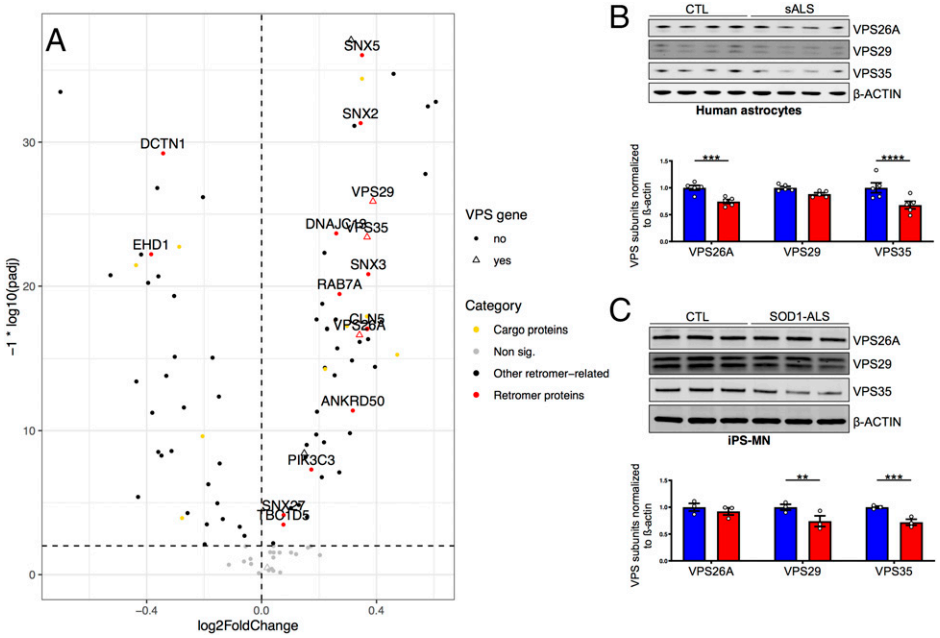

Fig. 1. Altered expression of retromer subunits in human ALS and control postmortem tissues and cell types. (*A*) Volcano plot showing retromer-related genes expressed in the postmortem spinal cord of 482 ALS compared with 118 healthy control samples. (*B*) Western blot analyses of VPS26A, VPS29, and VPS35 contents in human astrocytes from postmortem samples from five control subjects with no known neurological disease (CTL; blue) and five patients with sporadic amyotrophic lateral sclerosis (sALS; red). Data are means ± SEM analyzed by two-way ANOVA [disease as the main factor: $F_{(1,29)} = 26.53$, $P < 0.0001$] followed by a Sidak post hoc test. ***$P = 0.003$ VPS26a CTL vs. sALS; ****$P < 0.0001$ Vps35 CTL vs. sALS. (*C*) Western blot analyses of VPS26A, VPS29, and VPS35 contents in 14 DIV human MNs derived from iPSCs from three control subjects with no known neurological disease (CTL; blue) and three patients with mutSOD1 (SOD1-ALS; red). Data are means ± SEM analyzed by two-way ANOVA [genotype main factor: $F_{(1,17)} = 14.77$, $P = 0.002$] followed by a Sidak post hoc test. **$P = 0.016$ VPS29 CTL vs. SOD1-ALS; ***$P = 0.011$ VPS35 CTL vs. SOD1-ALS.

difference in spinal cord Vps35, Vps29, and Vps26a mRNA contents between Tg SOD1^{G93A} mice and age-matched nontransgenic (NTg) controls at any of the three selected time points (*SI Appendix*, Fig. S2 *A–C*). However, by reviewing the spatial transcriptomic data from Tg SOD1^{G93A} spinal cords (23), we found that Vps26a, Vps29, and Vps35 subunits showed regional differences that occurred within the spinal cord that were not detected in our qRT-PCR experiments (*SI Appendix*, Fig. S2 *D–G*). For instance, at presymptomatic stage prior to any overt loss of spinal MNs, there were higher levels of Vps26a, Vps29, and Vps35 mRNAs as well as of Snx27, which is important for the cell surface recycling of specific cargos (1), in the gray matter of Tg SOD1^{G93A} spinal cords compared with controls (*SI Appendix*, Fig. S2 *D–G*).

Next, we performed Western blot analyses on spinal cord lysates for Vps26a, Vps29, and Vps35 in Tg SOD1^{G93A} mice (Fig. 2) and their age-matched NTg controls. The analysis of these lysates showed no significant difference in protein levels at P60 and P90 (Fig. 2 *A* and *B*). However, the three cargo-selective subcomplex proteins were reduced in spinal cords of Tg SOD1^{G93A} mice compared with controls at P120 (Fig. 2*C*). In contrast to the reduction in cargo-selective subcomplex proteins, we found an increase in the membrane-bending subcomplex protein Snx1 and no change in Snx2 or Snx5 in spinal cords of Tg SOD1^{G93A} mice compared with controls at P120 (*SI Appendix*, Fig. S3*A*).

As for retromer cargos, we assessed glutamate ionotropic receptor α-amino-3-hydroxy-5-methyl-4-isoxazolepropionic acid 1 (GluA1, also called Gria1) and sortilin, which are retrogradely trafficked by the retromer to the cell surface and trans-Golgi network, respectively (1). Paralleling the changes in cargo-selective subcomplex proteins, we found a significant reduction of GluA1 protein levels in Tg SOD1^{G93A} spinal cords compared with controls (Fig. 2) but again, only at P120; of note, the spinal cord levels of GluA1 did correlate with the age-dependent decrease of Vps35 [$r_{(28)} = 0.41$, $P = 0.029$]. In contrast, we found a slight increase of sortilin proteins in Tg SOD1^{G93A} spinal cords compared with controls at P120 (*SI Appendix*, Fig. S3*A*). Thus, our findings suggest that the retromer is dysfunctional in Tg SOD1^{G93A} mice and that this alteration is associated with a trafficking defect of specific cargos.

To confirm that this retromer deficit that we observed in spinal cords from Tg SOD1^{G93A} mice was related to the mutant form of SOD1 and not merely to its overexpression, we examined retromer proteins in Tg mice overexpressing comparable levels of the wild-type SOD1 (SOD1^{wt}). At P120, control spinal cords from Tg SOD1^{wt} mice and age-matched NTg mice showed comparable levels of Vps26a, Vps29, and Vps35 proteins (*SI Appendix*, Fig. S3*B*). Given the ubiquitous expression of SOD1, we also assessed the level of the cargo-selective proteins in the cerebral cortex, cerebellum, and a nonneural tissue (kidney) in Tg SOD1^{G93A} and NTg mice by Western blot. We found, akin to the spinal cord albeit to a lesser extent, reductions in Vps35, Vps26A, and GluA1 protein contents in the cerebral cortex (Fig. 2*D*) and no significant reductions in the cerebellum of P120 Tg SOD1^{G93A} mice compared with age-matched NTg mice (*SI Appendix*, Fig. S3*C*). In contrast to neural tissues, none of the three retromer core protein contents were decreased in the kidney of P120 Tg SOD1^{G93A} mice (*SI Appendix*, Fig. S3*D*). Thus, the aforementioned findings suggest that there is an alteration in the retromer complex in neural tissues readily detectable in Tg SOD1^{G93A} mice close to end stage.

Altered Expression of Retromer Components in Tg SOD1^{G93A} MNs and Astrocytes. Next, we thought that it would be important to confirm that this retromer deficit was detectable in MNs from Tg SOD1^{G93A} mice. We assessed Vps35 in adult spinal cord sections of adult mice by immunofluorescence (Fig. 3*A*). The mean fluorescence for Vps35 in spinal MN expressing choline acetyltransferase (ChAT) was markedly lower in P120 Tg SOD1^{G93A} mice compared with age-matched NTg controls (Fig. 3*B*). Likewise, the mean fluorescence for Vps35 of neurons within the primary motor area expressing the corticospinal MN transcription factor CTIP2 (24) was also reduced in P120 Tg vs. NTg mice (*SI Appendix*, Fig. S3*E*); these cortical MNs were examined since they are also affected in ALS (15) and in this mouse model (25). Thus, these findings indicate that the reduction in Vps35 detected in the spinal cord lysates from Tg SOD1^{G93A} mice involves MNs. Yet, since the reduction in Vps35 immunoreactivity in MNs appeared to concern not only the diffuse cytosolic but also, the punctate fluorescence, we sought to compare the distribution and density of endosomes and their colocalization with Vps35 in Tg SOD1^{G93A} and NTg MNs. These analyses revealed that the number of the Vps35-positive punctate foci was indeed reduced in P120 Tg SOD1^{G93A} compared with NTg MNs but that their sizes were not significantly different between the two genotypes (*SI Appendix*, Fig. S4*A*). As for the EEA1-labeled early endosomes, Rab7a-labeled late endosomes, and Lamp1-labeled lysosomes (1), we found larger and fewer Rab7a-positive punctates in Tg SOD1^{G93A} vs. NTg MNs (*SI Appendix*, Fig. S4*C*). In both genotypes, the colocalization of Vps35 was highest with late endosomes followed by early endosomes and then, lysosomes (*SI Appendix*, Fig. S4). However, we found a relatively greater colocalization of Vps35 with early endosome antigen 1 (EEA1) punctates but an inverse trend with Ras-related protein Rab7a or Lamp1 in Tg SOD1^{G93A} vs. NTg MNs (*SI Appendix*, Fig. S4). These data suggest that while the endosomal association of Vps35 in MNs is reduced in this model of ALS, there appears to be a shift toward a greater association of Vps35 with early rather than late endosomes or lysosomes in Tg SOD1^{G93A} vs. NTg MNs.

We next assessed the expression of retromer subunits in Tg SOD1^{G93A} and NTg astrocytes. Mutant astrocytes displayed reduced Vps26a, Vps29, and Vps35 protein expression (Fig. 3 *C* and *D*), while mRNA levels remained unchanged as measured by qRT-PCR (*SI Appendix*, Fig. S5). Our results in Tg SOD1^{G93A} MNs and astrocytes replicate those observed in the mouse spinal cord and raised the possibility that the retromer defect stems from a posttranscriptional alteration. To begin to investigate this possibility, we compared degradation kinetics of the cargo-selective trimer by cycloheximide chase in cultured Tg SOD1^{G93A} and NTg mice astrocytes. This experiment revealed that, while initial Vps35 protein levels were lower in Tg SOD1^{G93A} compared with NTg astrocytes, Vps35 half-life did not differ between the two genotypes (Fig. 3 *E* and *F*); identical patterns were found for Vps29 and Vps26a. These results suggest that cargo-selective trimer degradation is not enhanced in ALS.

Overexpression of VPS35 in Tg SOD1^{G93A} Mice Worsens the Disease Phenotype. The convergence of retromer deficit from our studies in human cell types and postmortem tissue makes the Tg SOD1^{G93A} mouse model of ALS suitable to test retromer-based disease-modifying strategies. In keeping with this idea, we assessed the effect of adeno-associated virus (AAV)–mediated overexpressing VPS35 on the ALS-like phenotype since such gene therapy was previously shown to rescue the expression of retromer components and retromer functionality in AD (26). Accordingly, P1 Tg SOD1^{G93A} mice received intracerebroventricular (ICV) injections of AAV9 vectors expressing human VPS35 or control green fluorescent protein

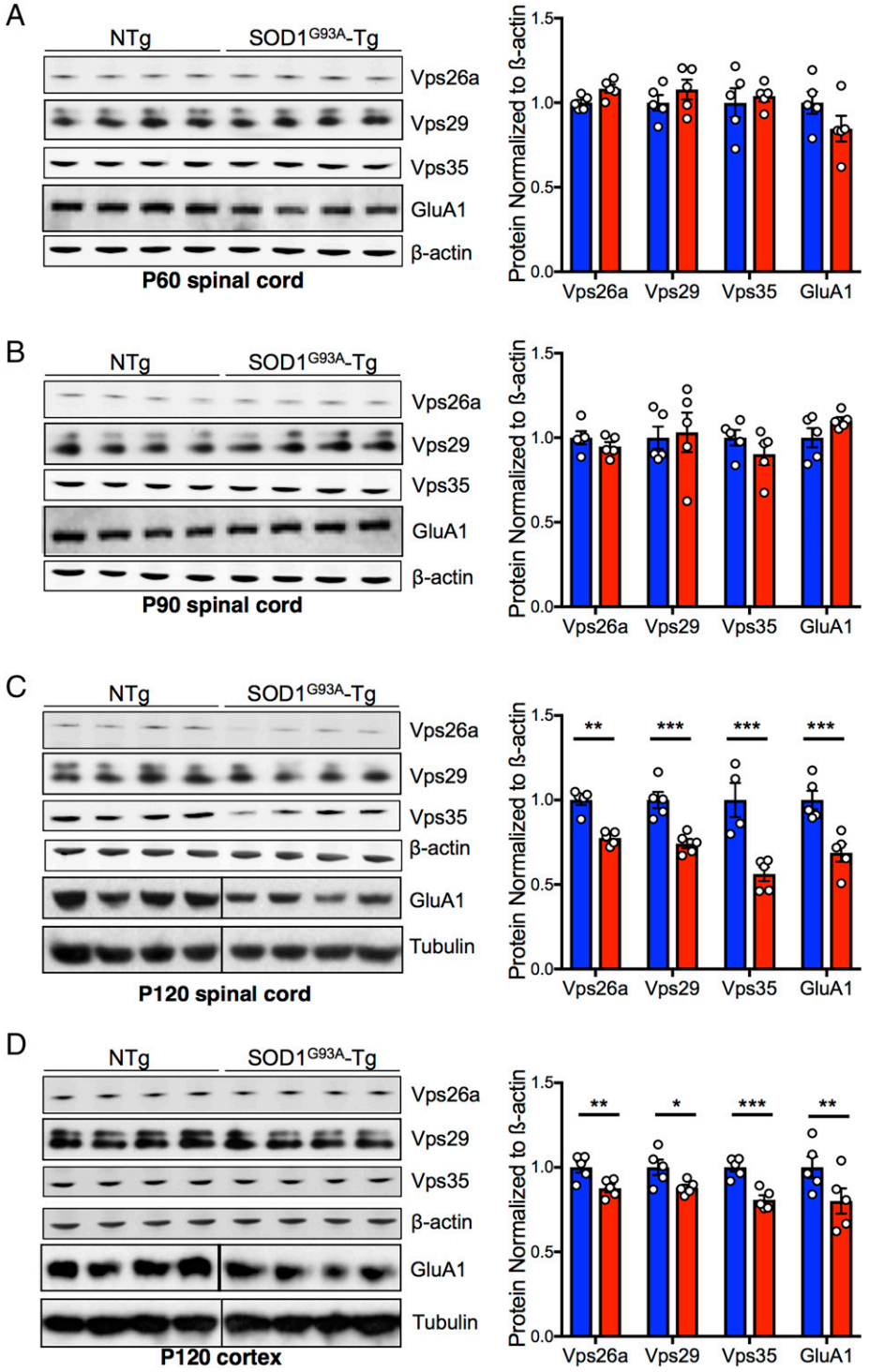

Fig. 2. Retromer core protein levels are decreased in neural tissues of Tg SOD1^{G93A} mice. (*A–C*) Western blots of Vps26a, Vps29, Vps35, and GluA1 on lysates from spinal cords of Tg SOD1^{G93A} mice (red; $n = 5$) and NTg littermates (blue; $n = 4$ to 5) at P60 (*A*), P90 (*B*), and P120 (*C*). Data are means ± SEM of independent experiments (n) analyzed by two-way ANOVA. (*A*) Genotype main factor: $F_{(1,39)} = 8.9E\text{-}3$, $P = 0.768$ followed by a Sidak post hoc test. (*B*) Genotype main factor: $F_{(1,39)} = 8.1E\text{-}3$, $P = 0.929$ followed by a Sidak post hoc test. (*C*) Genotype main factor: $F_{(1,38)} = 81.17$, $P < 0.001$ followed by a Sidak post hoc test. $^{**}P = 0.002$ Vps26a NTg vs. Tg; $^{***}P < 0.001$ Vps29, Vps35, and GluA1 NTg vs. Tg. (*D*) Western blots of Vps35, Vps26a, Vps29, and GluA1 on lysates from cerebral cortex of Tg SOD1^{G93A} mice (red; $n = 5$) and NTg littermates (blue; $n = 5$) at P120. (*D*) Genotype main factor: $F_{(1,39)} = 27.03$, $P < 0.001$ followed by a Sidak post hoc test. $^{***}P = 0.003$ Vps35 NTg vs. Tg, $^{**}P = 0.008$ Vps26a and GluA1 NTg vs. Tg and $^{*}P = 0.026$ Vps29 NTg vs. Tg.

(GFP) driven by the cytomegalovirus promotor. Transduction with AAV9-VPS35 rescued the expression of both Vps35 and other core components, such as Vps26a, to near NTg control levels (*SI Appendix*, Fig. S6*A*).

Following this gene therapy, we noted that the onset of disease manifestations in Tg SOD1^{G93A} mice did not significantly differ from that in AAV9-VPS35–injected animals (i.e., age at which Tg mice show a 10% loss of their maximal body weight) (Fig. 4*A*). However, AAV9-VPS35–injected Tg SOD1^{G93A} mice showed a faster decline in motor performance as assessed by the grip strength test compared with AAV9-GFP–injected Tg SOD1^{G93A} (Fig. 4*B*). Likewise, survival, as defined by the

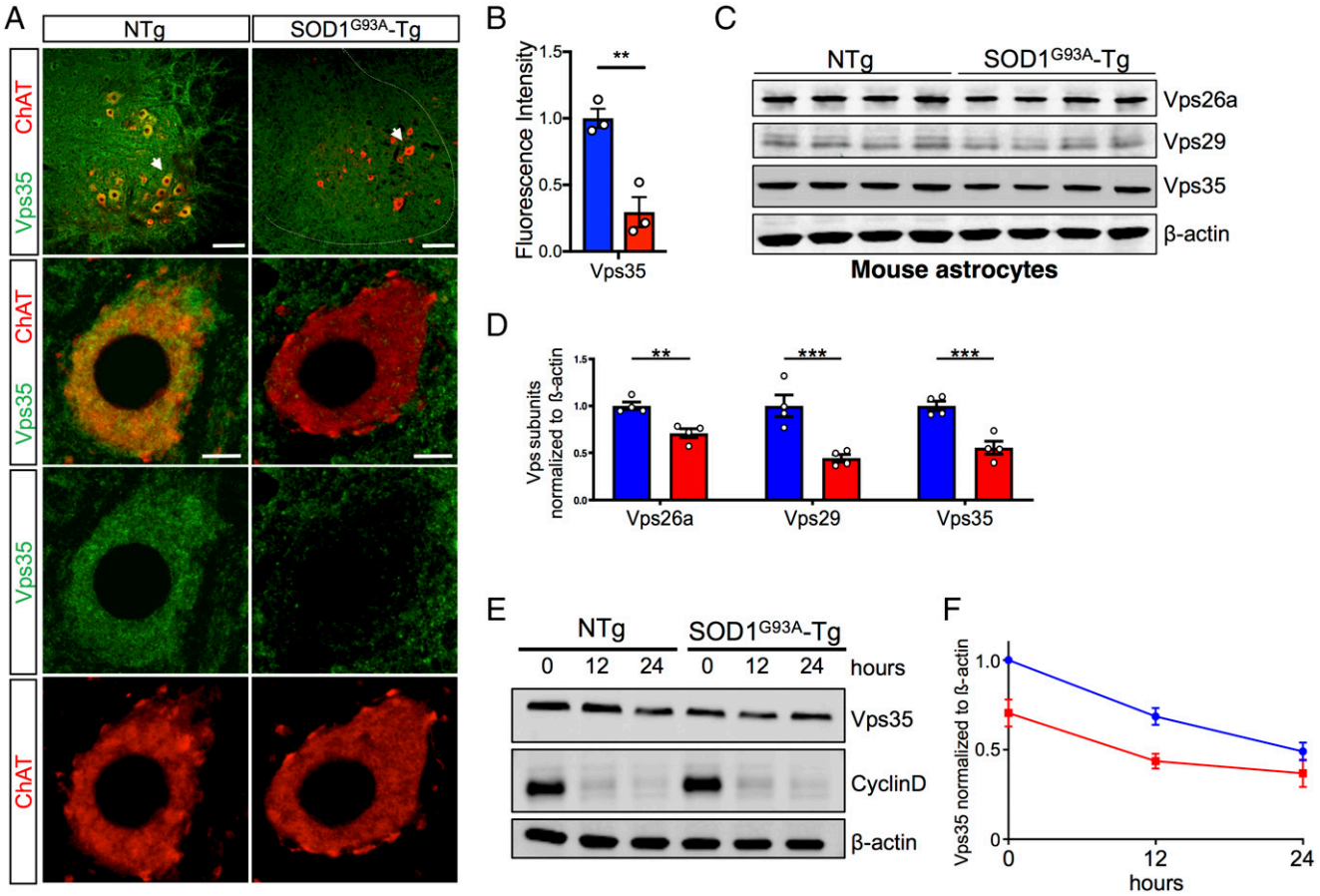

Fig. 3. Retromer proteins are reduced in neurons and astrocytes form Tg SOD1^{G93A} mice. (*A*) Representative images of 20-μm-thick L4/L5 spinal cord sections at low and high magnifications from a Tg SOD1^{G93A} mouse and an NTg littermate immunostained for Vps35 (green) and ChAT (red). (Scale bars: row 1, 125 μm; row 2, 10 μm.) (*B*) Quantification of corrected total cell Vps35 immunofluorescent signal in spinal MNs identified by ChAT immunostaining. Data are means ± SEM of three Tg (red) and NTg (blue) mice (three to five L4/L5 spinal MNs per mouse) compared by the two-tailed Student's *t* test: $t_{(4)} = 5.27$. $^{**}P = 0.0062$. (*C*) Western blot analyses of Vps26a, Vps29, and Vps35 contents in cultured mouse primary astrocytes from Tg SOD1^{G93A} mice (red) and NTg littermates (blue). (*D*) Quantification of *C*. Data are means ± SEM of four independent experiments analyzed by two-way ANOVA [genotype main factor: $F_{(1,23)} = 63.782$, $P < 0.001$] followed by a Sidak post hoc test. $^{**}P = 0.006$ Vps26a NTg vs. Tg; $^{***}P < 0.001$ Vps29 and Vps35 NTg vs. Tg. (*E*) Representative western blot analysis of Vps35 levels in mouse primary astrocytes treated with cycloheximide (CHX) at different time points; β-actin is used as the loading control. (*F*) Quantification of Vps35 CHX chase. Data are means ± SEM of four independent experiments using primary mouse Tg astrocytes (red) and NTg astrocytes (blue). The Y-intercept and half-life of Vps35 in the two genotypes were estimated by nonlinear fitting (*Materials and Methods*) and compared by the two-tailed Student's *t* test. The Y-intercept was significantly different between the two groups: $t_{(6)} = 3.43$, $P = 0.014$; half-life was not: $t_{(6)} = -0.72$, $P = 0.50$.

age at which these mice can no longer right themselves from a supine position within 30 s, was shorter in mice injected with AAV9-VPS35 (Fig. 4*C*). In keeping with the life span results, we found that P120 AAV9-VPS35–injected Tg SOD1^{G93A} mice showed lower counts of lumbar (L)4/L5 MN compared with AAV9-GFP–injected Tg SOD1^{G93A} mice (Fig. 4 *D*–*F*). Moreover, there was a trend toward greater glial response in P120 AAV9-VPS35–injected Tg SOD1^{G93A} mice compared with their AAV9-GFP–injected counterparts as suggested by an ∼23% higher ionized calcium-binding adapter molecule 1 (Iba1) signal in spinal cord lysates of the former compared with the latter (*SI Appendix*, Fig. S6*B*). The results demonstrate that, while VPS35 overexpression did improve retromer levels, this was associated with a worsening of the disease phenotype in Tg SOD1^{G93A} mice.

Heterozygous Null Vps35 Mutation in Tg SOD1^{G93A} Mice Delays Disease Expression. Given our findings of faster declines in strength and shortened survival of Tg SOD1^{G93A} mice overexpressing Vps35 in MNs, we reasoned that exacerbating the already lower levels of Vps35 might have a beneficial effect in this ALS mouse model. We thus generated Tg SOD1^{G93A} mice with a partial genetic deficiency in Vps35 by crossing first Vps35$^{Flox/Flox}$ with cytomegalovirus (CMV).Cre^{+} mice and their heterozygous Vps35-null mutant (Vsp35$^{+/-}$) progeny with Tg SOD1^{G93A} mice. It was previously shown that Vsp35$^{+/-}$ mice express lower levels of both Vps35 and Vps26a proteins throughout the central nervous system (27, 28). We confirmed this finding in our Vsp35$^{+/-}$;Tg SOD1^{G93A} mice (*SI Appendix*, Fig. S7*A*). Then, we ran a similar series of investigations in Vps35$^{+/-}$;Tg SOD1^{G93A} mice, like those done in AAV9-injected Tg SOD1^{G93A} mice. Strikingly, we found that the onset of the disease manifestations in Vps35$^{+/-}$;Tg SOD1^{G93A} mice was delayed in comparison with Vps35$^{+/+}$;Tg SOD1^{G93A} control animals (Fig. 5*A*). Likewise, there was a slower deterioration in motor performance (Fig. 5*B*) as well as a longer survival in Vps35$^{+/-}$;Tg SOD1^{G93A} mice (Fig. 5*C*). Furthermore, we found higher L4/L5 MN counts in P120 Vps35$^{+/-}$;Tg SOD1^{G93A} mice compared with age-matched control Vps35$^{+/+}$;Tg SOD1^{G93A} mice (Fig. 5 *D* and *E*). In keeping with this, there was a trend toward decreased glial response in Vps35$^{+/-}$;Tg SOD1^{G93A} vs. Vps35$^{+/+}$;Tg SOD1^{G93A} animals, as suggested by a ∼21% lower glial fibrillary acidic protein (GFAP) signal in spinal cord lysates from the former compared with the latter (*SI Appendix*, Fig. S7*B*).

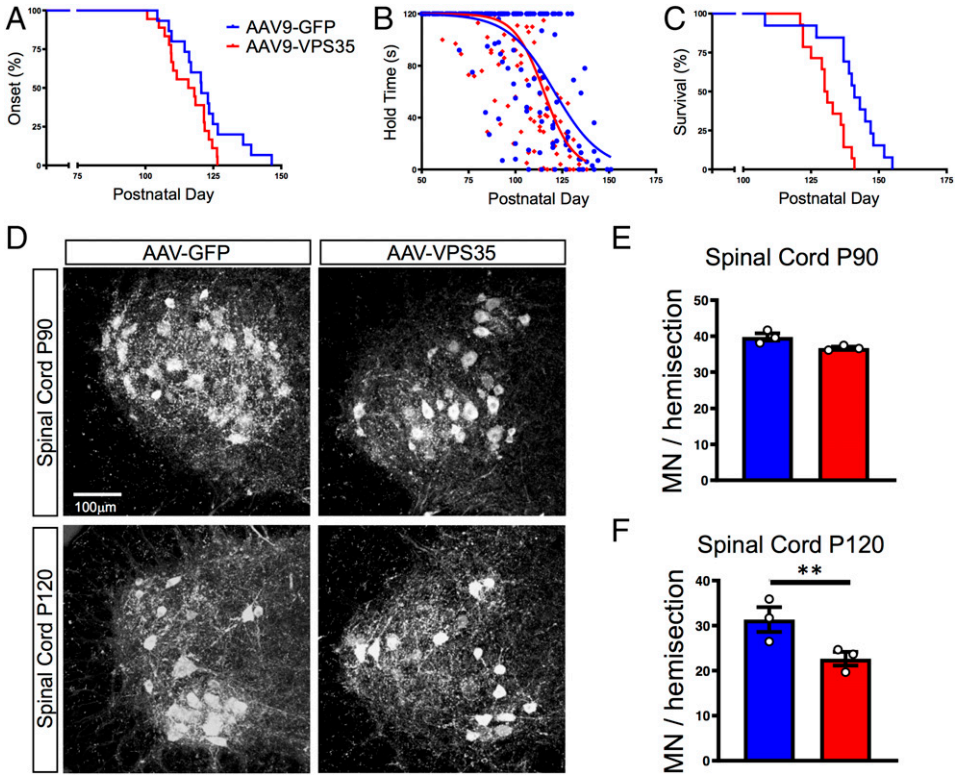

Fig. 4. VPS35 overexpression in Tg SOD1^{G93A} mice hastens the disease phenotype. Tg SOD1^{G93A} mice were injected ICV at P1 with either AAV9-VPS35 or AAV9-GFP. (*A*) Age at onset of the disease phenotype in Tg SOD1^{G93A} mice injected with AAV9-VPS35 (red; median: 116 d; $n = 18$) or AAV9-GFP (blue; median 121 d; $n = 15$) defined as the age at which a mouse loses 10% of its peak body weight. Log-rank Mantel–Cox test = 2.995, degrees of freedom 1, $P = 0.084$. (*B*) Inverted grid test performed weekly starting at P50. Data from Tg SOD1^{G93A} mice injected with AAV9-VPS35 (red; $n = 18$) or AAV9-GFP (blue; $n = 15$) were analyzed by the nonlinear regression curve fit and compared using the least sum of squares method [$F_{(2,536)} = 389.6$, $P < 0.0001$]. (*C*) Age at end stage of the disease phenotype in Tg SOD1^{G93A} mice injected with AAV9-VPS35 (median: 130 d; $n = 14$) or AAV9-GFP (median 141 d; $n = 13$) defined as the age at which a mouse can no longer right itself after 30 s when placed on its back. Log-rank Mantel–Cox test = 10.735, degrees of freedom 1, $P = 0.001$. (*D*) Representative images of 70-μm-thick L4/L5 ventral horn spinal cord hemisections from a P90 and P120 Tg SOD1^{G93A} mouse injected with AAV9-VPS35 (red) or AAV9-GFP (blue) immunostained for ChAT. (Scale bar: 100 μm.) (*E* and *F*) ChAT-immunostained neurons in each ventral horn hemisection were manually counted under fluorescent microscopy. Data are means ± SEM of $n = 3$ mice per genotype and time point and were analyzed by two-way ANOVA [virus main factor: $F_{(1,11)} = 12.594$, $P = 0.008$] followed by a Sidak post hoc test. **$P = 0.006$ P120 NTg vs. Tg.

Meta-Analysis of Whole-Genome and Exome Sequencing for Enrichment of Retromer-Related Genes in ALS. Since overexpression of VPS35 in mutSOD1 Tg mice exacerbated the ALS-like phenotype and further depletion led to disease mitigation, we investigated whether LOF variants in the HRCGS were inversely associated with ALS risk. We reanalyzed the variant count tables of two publicly available datasets: a whole-genome sequencing (WGS) cohort, which included 4,366 patients with ALS and 1,832 healthy controls (29), and a whole-exome sequencing (WES) cohort, which included 2,874 patients with ALS and 6,405 controls (30). While both WGS and WES cohorts showed clear LOF enrichment in *NEK1* in ALS cases (as published in both cohorts), no gene in the HRCGS showed significant LOF depletion in ALS (or enrichment in controls). In each cohort, the top enriched gene in this set did not even show nominal significance (WES cohort, *TF* gene $P = 0.055$; WGS cohort, *STAM* gene $P = 0.054$). No gene from the HRCGS showed statistically significant enrichment/depletion in other classes of mutations, including coding variants that were predicted to harm protein function, or all coding variants.

Although individual retromer genes did not show an enrichment or depletion, we assessed if genes in the HRCGS were more likely than other genes to show enrichment of LOF variants in controls. In the WES cohort, where a gene set burden test was not possible with the available data, the opposite proved true; 65% of genes in this set showed more LOF variants in patients with ALS (38 of 58) compared with 50% of non-HRCGS genes (4,892 of 9,758). Although this difference in proportions was nominally significant (uncorrected $P = 0.02$), we did not see this effect in the equivalent analysis in the WGS cohort, where the proportion of HRCGS genes with more variants in ALS patients was indistinguishable from non-HRCGS genes (54% or 30 of 56 vs. 52% or 4,151 of 8,017, $P = 0.089$). Because the WES variant tables included only extremely rare variants, we could approximate the proportion of individuals in ALS patients and controls carrying an LOF mutation in any gene of the HRCGS. This proportion of ALS subjects with mutations (2.96%, 85 of 2,874) did not differ from controls (2.67%, 171 of 6,405, $P = 0.48$). Thus, based on these cohorts, there is no genetic evidence that depletion of the LOF mutation in retromer genes is a strong risk factor for developing ALS.

Discussion

Dysfunction in retromer, a multimodular protein assembly that recycles transmembrane proteins out of the endosomal compartment (1), has been identified in a growing number of neurodegenerative diseases (3–6). In keeping with this, the present study reports on three key observations relevant to the status of the retromer in the common neurodegenerative MN disease ALS. First, we found a reduction in the expression of all three core cargo-selective subcomplex proteins of the retromer in neural tissues of symptomatic Tg SOD1^{G93A} mice and have demonstrated that this deficit is associated with decreased levels of the GluA1 protein, which is

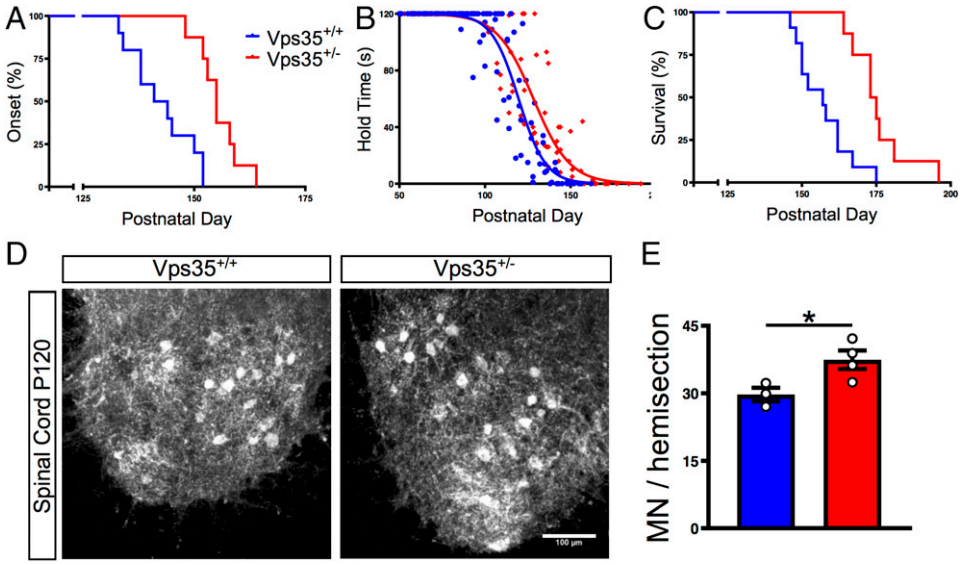

Fig. 5. Heterozygous deletion of Vps35 in Tg SOD1^{G93A} mice attenuates the disease phenotype. Mice were bred to express the SOD1^{G93A} transgene and either a single Vps35 null allele (Vps35$^{+/-}$) or wild-type Vps35 (Vps35$^{+/+}$). (*A*) Age at onset of the disease phenotype in Vps35$^{+/-}$;Tg SOD1^{G93A} mice (red; median: 155 d; $n = 8$) and Vps35$^{+/+}$;Tg SOD1^{G93A} mice (blue; median 144 d; $n = 10$) defined as the age at which a mouse loses 10% of its peak body weight. Log-rank Mantel–Cox test = 12.408, degrees of freedom 1, $P < 0.0001$. (*B*) Inverted grid test performed weekly starting at P50. Data from Vps35$^{+/-}$;Tg SOD1^{G93A} mice (red; $n = 7$) and Vps35$^{+/+}$;Tg SOD1^{G93A} mice (blue; $n = 7$) were analyzed by the nonlinear regression curve fit and compared using the least sum of squares method [$F_{(2,222)} = 19.28$, $P < 0.0001$]. (*C*) Age at end stage of the disease phenotype in Vps35$^{+/-}$;Tg SOD1^{G93A} mice (red; median: 173 d; $n = 8$) or Vps35$^{+/+}$;Tg SOD1^{G93A} mice (blue; median 157 d; $n = 11$) defined as the age at which a mouse can no longer right itself after 30 s when placed on its back. Log-rank Mantel–Cox test = 10.197, degrees of freedom 1, $P = 0.001$. (*D*) Representative images of 70-µm-thick L4/L5 ventral horn spinal cord hemisections from P120 Vps35$^{+/-}$;Tg SOD1^{G93A} and Vps35$^{+/+}$;Tg SOD1^{G93A} mice immunostained for ChAT. (Scale bar: 100 µm.) (*E*) ChAT-immunostained neurons in each ventral horn hemisection were manually counted under fluorescent microscopy. Data are means ± SEM of $n = 4$ Vps35$^{+/-}$;Tg SOD1^{G93A} (red) and $n = 3$ Vps35$^{+/+}$;Tg SOD1^{G93A} (blue) mice and were analyzed by two-tailed Student's *t* test. *$t_{(5)} = -2.821$, $P = 0.037$.

communally used as a functional readout of the retromer. Second, to better define the cellular origin of the retromer defect observed in whole tissues, our investigations revealed that expression of core retromer subunits is reduced in both neuronal and nonneuronal cells, such as spinal MNs and astrocytes. Third, expanding our results into humans, we show that both iPSC-derived MNs and primary astrocytes from patients with ALS show comparable decreases in the retromer expression as seen in the Tg mouse model of ALS. Therefore, our findings together with those of Muzio et al. (14) provide compelling evidence supporting a deficit in the retromer in ALS through a broad set of independent investigations resting on both in vitro and in vivo studies in mouse and human cells and tissues.

The deficit in the retromer in neurodegenerative disorders may be genetic in nature due to pathogenic mutations in core retromer subunits, such as in PD (11, 13), or allelic variants for retromer-related factors, like those associated with a greater risk of developing AD (31–33). Mutations in these same genes have not yet been linked to ALS by several large whole-genome/exome studies (29, 30) nor by genome-wide association studies. Although a spontaneous mouse mutation in *Vps54*, a Golgi-associated retrograde protein complex subunit, causes MN degeneration leading to progressive muscle weakness in mice with similarities to ALS (34), no mutations in *VPS54* or any components of the Golgi-associated retrograde protein complex have been associated with ALS in humans (35). Collectively, this information strongly argues against the idea that the retromer deficit documented by our study and the work of Muzio et al. (14) stems from a genetic defect. Moreover, in contrast to previous reports in AD and PD (3, 9–13), in none of our investigations done in ALS samples did we find evidence that the reported retromer deficit was associated with reduction in mRNA levels for the different retromer core subunits. This is similar to the mRNA data from Muzio et al. (14) in ALS, and from Vagnozzi et al. (6) in two other neurodegenerative disorders, namely Pick's disease and progressive supranuclear palsy. These findings support that the source of the defect in ALS and perhaps, other neurodegenerative disorders originates from alterations at the posttranscriptional level and in particular in light of our findings of the unaltered half-life of Vps35 in mouse mutSOD1-expressing astrocytes, at the translational level. This interpretation is particularly appealing given the growing recognition of the pathogenic role of altered RNA metabolism in a variety of diseases of the nervous system, including ALS (36, 37), and calls for additional future investigations. Of note, in our hands, the retromer deficiency was only detected in symptomatic mice, suggesting that retromer deficit coincides with the degeneration of spinal MNs and the ensuing glial response (38, 39). This finding is in contrast to that of Muzio et al. (14), which reports a reduction in Vps35 in spinal cord from Tg SOD1^{G93A} mice as early as P20. If their results are confirmed, retromer deficit would be among the earliest known molecular alteration in Tg SOD1^{G93A} mice with signs of endoplasmic reticulum stress and of MN electrophysiological changes (40). Despite this temporal discrepancy, both our study and the study of Muzio et al. (14) agree on the potential pathogenic significance of retromer deficit in ALS.

Retromer deficiencies have almost uniformly been found to have deleterious effects on disease. The work of Muzio et al. (14) would indicate that the same is true in ALS. Yet, our findings using gene therapy rather than a pharmacological approach to rescue the retromer deficit in Tg SOD1^{G93A} mice led to accelerated clinical and MN deterioration. While pharmacological chaperones have the benefit of targeting the retromer complex proteins already found in the cell, they, like all drugs, have the potential of having off-target effects. Conversely, viral-mediated expression, which has been studied as a form of retromer repletion, is less likely to provoke such spurious effects.

However, it carries the risk of itself being cytotoxic by introducing exogenous excessive amounts of core proteins into the retromer machinery, which in turn, may affect proteostasis. Relevant to this view is the work of Munsie et al. (41) showing that overexpression of VPS35 can be neurotoxic. Worth noting, the deleterious effect of overexpression gene therapy was also observed by Van Alstyne et al. (42) upon attempting to rescue the survival motor neuron complex with a viral vector in a mouse model of another MN disease called spinal muscle atrophy. Thus, rescue strategies for protein complexes may be fraught with safety challenges related to the ensuing supraphysiological, uncontrolled expression of the exogenous gene product.

Given the outcomes of our overexpression study, we sought to assess the effect of Vps35 haploinsufficiency in Tg SOD1^{G93A} mice, which revealed an attenuation of the disease phenotype in this mouse model of ALS. Considering these findings, we propose that alteration in retromer—by unevenly affecting cargos with different functions in both neurons and glia—may have disparate and even opposite biological consequences. Supporting this view, herein we found a reduction in spinal cord contents of the retromer cargo GluA1, a change that can be neuroprotective by attenuating the glutamate-mediated excitotoxic tone on spinal MNs; of note, excitotoxicity is a major pathogenic hypothesis in ALS (43). Also relevant to the role of retromer in ALS are noncell autonomous scenarios that pertain to the processing of amyloid precursor protein (APP) and of lipid droplets in astrocytes. Indeed, we have reported that astrocyte-generated fragments of APP, whose processing and trafficking rely on retromer (1), contribute to spinal MN degeneration (44), whereas Moulton et al. (45) have shown that the knockdown of Vps35 impairs the formation of lipid droplets in astrocytes, which in turn, abrogates protection against the neurotoxicity of peroxidated lipids. Consequently, while a profound impairment of retromer function may be harmful, including to MNs (46), a lesser reduction may have an unattended effect of being beneficial, at least in ALS. The corollary is that therapies aimed at increasing retromer expression in ALS may not have the surmised disease-modifying effects, hence warranting further preclinical investigations prior to embarking on human clinical trials.

Materials and Methods

Animals. All procedures involving mice were approved by the Institutional Animal Care and Use Committee of Columbia University. Tg SOD1^{G93A} and SOD1^{wt} (C57BL/6J or B6SJL) were obtained from the Jackson Laboratory (stock nos. 004435 and 002726), and the Vps35-floxed mice were produced by the Center for Mouse Genome Modification at UConn Health (University of Connecticut) and have been described in Simoes et al. (28). CMV-Cre mice were obtained from the Jackson Laboratory (stock no. 006054) and have been described in Schwenk et al. (47). Further information is available in *SI Appendix, Supplementary Text*.

Western Blotting. All western blot analyses were performed on mouse tissues and cultured cells as in ref. 48 using the following primary antibodies: Vps26a (1:2,000, ab23892; Abcam), Vps29 (1:1,000, SAB2501105; Sigma), Vps35 (1:1,000, ab57632; Abcam), GluA1 (1:1,000, MAB2263; Sigma), SNX1 (1:1,000, 10304; Proteintech), SNX2 (1:1,000, HPA037400; Sigma), SNX5 (1:1,000, 17918; Proteintech), Sortilin (1:2,000, ab263864; Abcam), IBA1 (1:500, 016-20001; WAKO), GFAP (1:5,000, 12389; Cell Signaling), α-tubulin (1:5,000, T6199; Sigma), and β-actin (1:40,000, ab476744; Abcam). Further information is available in *SI Appendix, Supplementary Text*.

Cycloheximide Chase Western Blot. This was performed as described in *SI Appendix, Supplementary Text* using mouse primary astrocytes from NTg and Tg SOD1^{G93A} pups.

qRT-PCR. This was performed as described in *SI Appendix, Supplementary Text* using a three-step real-time qPCR that was conducted as in ref. 48 with the QuantStudio 3 Real-Time PCR System (Applied Biosystems) using SYBR Green dye (4367659; ThermoFisher).

iPSCs. iPSCs from three independent ALS patients with mutSOD1 and three independent healthy controls were provided by the Columbia Stem Cell Core and the laboratory of Michael Boland. iPSCs were maintained and differentiate to MNs as in ref. 48. At 14 DIV, iPSC-derived MNs were collected for experiments. Further information is available in *SI Appendix, Supplementary Text*.

Primary Astrocyte Culture. Tg SOD1^{G93A} and NTg primary astrocytes were from P3 mice prepared and cultured as previously described (49). Human astrocytes cultures were collected as previously described (50, 51) and maintained in astrocyte media.

Immunohistochemistry of Spinal Cord and Motor Cortex. This was performed as described in *SI Appendix, Supplementary Text* using primary antibodies against VPS35 (1:50, ab10099; Abcam) and CTIP2 (1:200, ab18465; Abcam) for brain and ChAT antibody (1:250, AB144P; Sigma) for spinal cord. Some spinal cord sections were also coimmunostained for VPS35, ChAT, EEA1 (1:100, 3288S; Cell Signaling), Rab7a (1:100, 9367S; Cell Signaling), or Lamp1 (1:100, 1D4B-S; DSHB). Images were quantified with ImageJ software (Research Resource Identifier [RRID]: SCR_003070) and Imaris software (RRID: SCR_007370).

AAV9 Transduction. AAV9s were produced by Virovek and injected ICV with 1×10^{11} viral particles following the protocol routinely used in our laboratory (52). Further information is available in *SI Appendix, Supplementary Text*.

Inverted Grid Test. The motor test of Oliván et al. (53) is routinely used in the laboratory with the minor modifications outlined in ref. 48. In brief, for this test, mice were placed on a grid and allowed to grip it with all four limbs. Further information is available in *SI Appendix, Supplementary Text*.

Spinal Cord MN Quantification. This was done as described in *SI Appendix, Supplementary Text*.

RNA-Seq Data Processing and Analysis. Stranded ribosomal ribonucleic acid-depleted RNA-seq data from the NYGC ALS Consortium spinal cord samples, processed as in ref. 54, were chosen to be analyzed. Cases were limited to those in the subject group "ALS Spectrum MND" ($n = 566$), and controls were limited to those in group "Non-Neurological Control" ($n = 118$). Dataset S1 has the list of samples with metadata, and *SI Appendix, Supplementary Text* has further detailed information.

Whole-Exome/Genome Analysis. This was done as described in *SI Appendix, Supplementary Text* using whole-exome data for individual genes; genetic models were obtained from supplementary table 6 from Cirulli et al. (30), while whole-genome data were downloaded from databrowser.projectmine.com/ (Data Freeze 1, ProjectMinE.Transcripts.ExAC.txt) (29, 55).

Statistical Analyses. All datasets are mean ± SEM, unless stated otherwise, of the number of biological replicates indicated in the figures run in two to three technical replicates as reported in ref. 48. All analyses were done with the GraphPad Prism V9 software (RRID: SCR_002798) with a rejection of the null hypothesis set at 0.05. Further information is available in *SI Appendix, Supplementary Text*.

Data Availability. All study data are included in the article and/or supporting information.

ACKNOWLEDGMENTS. We thank Scott Small, Clarissa Waites, Neil Shneider, Carol Troy, and Matthew Farrer for their support and critical comments on this work; Theresa Swayne for her invaluable help and guidance with the Imaris Software use; and James Caicedo and Norma Romero for technical expertise. E.J.P.-T. is supported by NIH, National Institute of Neurological Disorders and Stroke F31 Individual National Research Service Award for Diverse PhD Students NS101966 as well as NIH T32 Institutional Training Grant GM007367. S.P. is supported by NIH Grants NS107442, NS117583, NS111176, and AG064596; United States Department of Defense Grant W81XWH-22-1-0127; the Parkinson Foundation; the Ludwig Foundation; and Project-ALS. All NYGC ALS Consortium activities are supported by ALS Association Grant 15-LGCA-234 and the Tow Foundation. This work used the resources of the Herbert Irving Comprehensive Cancer Center Confocal and Specialized Microscopy Shared Resource funded in part through Center Grant P30CA013696.

1. M. N. J. Seaman, The retromer complex: From genesis to revelations. *Trends Biochem. Sci.* **46**, 608–620 (2021).
2. F. L. Tang *et al.*, VPS35 deficiency or mutation causes dopaminergic neuronal loss by impairing mitochondrial fusion and function. *Cell Rep.* **12**, 1631–1643 (2015).
3. S. A. Small *et al.*, Model-guided microarray implicates the retromer complex in Alzheimer's disease. *Ann. Neurol.* **58**, 909–919 (2005).
4. Y. Zhao *et al.*, Reduced LRRK2 in association with retromer dysfunction in post-mortem brain tissue from LRRK2 mutation carriers. *Brain* **141**, 486–495 (2018).
5. X. Wang *et al.*, Loss of sorting nexin 27 contributes to excitatory synaptic dysfunction by modulating glutamate receptor recycling in Down's syndrome. *Nat. Med.* **19**, 473–480 (2013).
6. A. N. Vagnozzi *et al.*, VPS35 regulates tau phosphorylation and neuropathology in tauopathy. *Mol. Psychiatry* **26**, 6992–7005 (2019).
7. J. Chu, D. Praticò, The retromer complex system in a transgenic mouse model of AD: Influence of age. *Neurobiol. Aging* **52**, 32–38 (2017).
8. D. A. MacLeod *et al.*, RAB7L1 interacts with LRRK2 to modify intraneuronal protein sorting and Parkinson's disease risk. *Neuron* **77**, 425–439 (2013).
9. E. Zavodszky *et al.*, Mutation in VPS35 associated with Parkinson's disease impairs WASH complex association and inhibits autophagy. *Nat. Commun.* **5**, 3828 (2014).
10. I. J. McGough *et al.*, Retromer binding to FAM21 and the WASH complex is perturbed by the Parkinson disease-linked VPS35(D620N) mutation. *Curr. Biol.* **24**, 1670–1676 (2014).
11. C. Vilariño-Güell *et al.*, VPS35 mutations in Parkinson disease. *Am. J. Hum. Genet.* **89**, 162–167 (2011).
12. J. Follett *et al.*, The Vps35 D620N mutation linked to Parkinson's disease disrupts the cargo sorting function of retromer. *Traffic* **15**, 230–244 (2014).
13. A. Zimprich *et al.*, A mutation in VPS35, encoding a subunit of the retromer complex, causes late-onset Parkinson disease. *Am. J. Hum. Genet.* **89**, 168–175 (2011).
14. L. Muzio *et al.*, Retromer stabilization results in neuroprotection in a model of amyotrophic lateral sclerosis. *Nat. Commun.* **11**, 3848 (2020).
15. L. P. Rowland, H. Mitsumoto, S. Przedborski, "Amyotrophic lateral sclerosis, progressive muscular atrophy and primary lateral sclerosis" in *Merritt's Neurology*, L. P. Rowland, T. A. Pedley, Eds. (Lippincott, Williams & Wilkins, Philadelphia, PA, 2010), chap. 128, pp. 802–808.
16. V. L. Feigin *et al.*; GBD 2016 Neurology Collaborators, Global, regional, and national burden of neurological disorders, 1990-2016: A systematic analysis for the Global Burden of Disease Study 2016. *Lancet Neurol.* **18**, 459–480 (2019).
17. G. Logroscino *et al.*; GBD 2016 Motor Neuron Disease Collaborators, Global, regional, and national burden of motor neuron diseases 1990-2016: A systematic analysis for the Global Burden of Disease Study 2016. *Lancet Neurol.* **17**, 1083–1097 (2018).
18. M. Nagai, H. Kikuchi, S. Przedborski, "Experimental models of motor neuron diseases" in *Amyotrophic Lateral Sclerosis*, H. Mitsumoto, S. Przedborski, P. H. Gordon, Eds. (Taylor & Francis, New York, NY, 2006), chap. 24, pp. 525–549.
19. A. C. M. Van Harten, H. Phatnani, S. Przedborski, Non-cell-autonomous pathogenic mechanisms in amyotrophic lateral sclerosis. *Trends Neurosci.* **44**, 658–668 (2021).
20. D. B. Re *et al.*, Necroptosis drives motor neuron death in models of both sporadic and familial ALS. *Neuron* **81**, 1001–1008 (2014).
21. H. Chen *et al.*, Modeling ALS with iPSCs reveals that mutant SOD1 misregulates neurofilament balance in motor neurons. *Cell Stem Cell* **14**, 796–809 (2014).
22. Y. Maury *et al.*, Combinatorial analysis of developmental cues efficiently converts human pluripotent stem cells into multiple neuronal subtypes. *Nat. Biotechnol.* **33**, 89–96 (2015).
23. S. Maniatis *et al.*, Spatiotemporal dynamics of molecular pathology in amyotrophic lateral sclerosis. *Science* **364**, 89–93 (2019).
24. P. Arlotta *et al.*, Neuronal subtype-specific genes that control corticospinal motor neuron development in vivo. *Neuron* **45**, 207–221 (2005).
25. P. H. Ozdinler *et al.*, Corticospinal motor neurons and related subcerebral projection neurons undergo early and specific neurodegeneration in hSOD1G^{93}A transgenic ALS mice. *J. Neurosci.* **31**, 4166–4177 (2011).
26. J. G. Li, J. Chiu, D. Praticò, Full recovery of the Alzheimer's disease phenotype by gain of function of vacuolar protein sorting 35. *Mol. Psychiatry* **25**, 2630–2640 (2020).
27. F. L. Tang *et al.*, VPS35 in dopamine neurons is required for Endosome-to-Golgi retrieval of Lamp2a, a receptor of chaperone-mediated autophagy that is critical for α-synuclein degradation and prevention of pathogenesis of Parkinson's disease. *J. Neurosci.* **35**, 10613–10628 (2015).
28. S. Simoes *et al.*, Tau and other proteins found in Alzheimer's disease spinal fluid are linked to retromer-mediated endosomal traffic in mice and humans. *Sci. Transl. Med.* **12**, eaba6334 (2020).
29. R. A. A. van der Spek *et al.*; Project MinE ALS Sequencing Consortium, The project MinE databrowser: Bringing large-scale whole-genome sequencing in ALS to researchers and the public. *Amyotroph. Lateral Scler. Frontotemporal Degener.* **20**, 432–440 (2019).
30. E. T. Cirulli *et al.*; FALS Sequencing Consortium, Exome sequencing in amyotrophic lateral sclerosis identifies risk genes and pathways. *Science* **347**, 1436–1441 (2015).
31. B. N. Vardarajan *et al.*, Identification of Alzheimer disease-associated variants in genes that regulate retromer function. *Neurobiol. Aging* **33**, 2231.e15–2231.e30 (2012).
32. B. N. Vardarajan *et al.*, Coding mutations in SORL1 and Alzheimer disease. *Ann. Neurol.* **77**, 215–227 (2015).
33. C. Reitz *et al.*; Alzheimer's Disease Genetics Consortium (ADGC), Independent and epistatic effects of variants in VPS10-d receptors on Alzheimer disease risk and processing of the amyloid precursor protein (APP). *Transl. Psychiatry* **3**, e256 (2013).
34. T. Schmitt-John *et al.*, Mutation of Vps54 causes motor neuron disease and defective spermiogenesis in the wobbler mouse. *Nat. Genet.* **37**, 1213–1215 (2005).
35. M. H. Meisler *et al.*, Evaluation of the Golgi trafficking protein VPS54 (wobbler) as a candidate for ALS. *Amyotroph. Lateral Scler.* **9**, 141–148 (2008).
36. J. K. Nussbacher, R. Tabet, G. W. Yeo, C. Lagier-Tourenne, Disruption of RNA metabolism in neurological diseases and emerging therapeutic interventions. *Neuron* **102**, 294–320 (2019).
37. Z. Butti, S. A. Patten, RNA dysregulation in amyotrophic lateral sclerosis. *Front. Genet.* **9**, 712 (2019).
38. L. Nardo *et al.*, Fluorimetric detection of the earliest events in amyloid β oligomerization and its inhibition by pharmacologically active liposomes. *Biochim. Biophys. Acta* **1860**, 746–756 (2016).
39. S. Vinsant *et al.*, Characterization of early pathogenesis in the SOD1(G93A) mouse model of ALS. Part I. Background and methods. *Brain Behav.* **3**, 335–350 (2013).
40. K. C. Kanning, A. Kaplan, C. E. Henderson, Motor neuron diversity in development and disease. *Annu. Rev. Neurosci.* **33**, 409–440 (2010).
41. L. N. Munsie *et al.*, Retromer-dependent neurotransmitter receptor trafficking to synapses is altered by the Parkinson's disease VPS35 mutation p.D620N. *Hum. Mol. Genet.* **24**, 1691–1703 (2015).
42. M. Van Alstyne *et al.*, Gain of toxic function by long-term AAV9-mediated SMN overexpression in the sensorimotor circuit. *Nat. Neurosci.* **24**, 930–940 (2021).
43. S. Vucic, J. D. Rothstein, M. C. Kiernan, Advances in treating amyotrophic lateral sclerosis: Insights from pathophysiological studies. *Trends Neurosci.* **37**, 433–442 (2014).
44. V. Mishra *et al.*, Systematic elucidation of neuron-astrocyte interaction in models of amyotrophic lateral sclerosis using multi-modal integrated bioinformatics workflow. *Nat. Commun.* **11**, 5579 (2020).
45. M. J. Moulton *et al.*, Neuronal ROS-induced glial lipid droplet formation is altered by loss of Alzheimer's disease-associated genes. *Proc. Natl. Acad. Sci. U.S.A.* **118**, e2112095118 (2021).
46. D. Sargent *et al.*, Neuronal VPS35 deletion induces spinal cord motor neuron degeneration and early post-natal lethality. *Brain Commun.* **3**, fcab208 (2021).
47. F. Schwenk, U. Baron, K. Rajewsky, A cre-transgenic mouse strain for the ubiquitous deletion of loxP-flanked gene segments including deletion in germ cells. *Nucleic Acids Res.* **23**, 5080–5081 (1995).
48. E. J. Pérez-Torres, "Retromer deficiency in amyotrophic lateral sclerosis," PhD thesis, Columbia University, New York, NY (2020).
49. M. Nagai *et al.*, Astrocytes expressing ALS-linked mutated SOD1 release factors selectively toxic to motor neurons. *Nat. Neurosci.* **10**, 615–622 (2007).
50. C. J. De Groot *et al.*, Establishment of human adult astrocyte cultures derived from postmortem multiple sclerosis and control brain and spinal cord regions: Immunophenotypical and functional characterization. *J. Neurosci. Res.* **49**, 342–354 (1997).
51. K. Abe *et al.*; Edaravone ALS Study Group, Confirmatory double-blind, parallel-group, placebo-controlled study of efficacy and safety of edaravone (MCI-186) in amyotrophic lateral sclerosis patients. *Amyotroph. Lateral Scler. Frontotemporal Degener.* **15**, 610–617 (2014).
52. C. M. Simon *et al.*, Stasimon contributes to the loss of sensory synapses and motor neuron death in a mouse model of spinal muscular atrophy. *Cell Rep.* **29**, 3885–3901.e5 (2019).
53. S. Oliván *et al.*, Comparative study of behavioural tests in the SOD1G93A mouse model of amyotrophic lateral sclerosis. *Exp. Anim.* **64**, 147–153 (2015).
54. O. H. Tam *et al.*; NYGC ALS Consortium, Postmortem cortex samples identify distinct molecular subtypes of ALS: Retrotransposon activation, oxidative stress, and activated glia. *Cell Rep.* **29**, 1164–1177.e5 (2019).
55. Project MinE ALS Sequencing Consortium, Project MinE: Study design and pilot analyses of a large-scale whole-genome sequencing study in amyotrophic lateral sclerosis. *Eur. J. Hum. Genet.* **26**, 1537–1546 (2018).